HETEROCYCLES, Vol. 102, No. 3, 2021, pp. 534 - 545. © 2021 The Japan Institute of Heterocyclic Chemistry
Received, 23rd December, 2020, Accepted, 22nd January, 2021, Published online, 29th January, 2021
DOI: 10.3987/COM-20-14401

STEPWISE REACTIONS BETWEEN CYCLIC 1,4-DIAZADIENES AND KETENES: CHARACTERISTICS AND MECHANISM

Kazuhide Nakahara,[a]* Koki Yamaguchi,[b] and Hisao Kansui[c]

[a] Department of Integrative Pharmaceutical Sciences, Faculty of Pharmaceutical Sciences, Setsunan University, 45-1 Nagaotoge-cho, Hirakata, Osaka 573-0101, Japan; E-mail address; kazuhide.nakahara@pharm.setsunan.ac.jp, [b] Laboratory of Molecular Design, Faculty of Pharmaceutical Sciences, Sojo University, 4-22-1 Ikeda, Nishi-ku, Kumamoto 860-0082, Japan, [c] Laboratory of Organic Chemistry, Faculty of Pharmaceutical Sciences, Sojo University, 4-22-1 Ikeda, Nishi-ku, Kumamoto 860-0082, Japan

Abstract – The reaction of unsymmetrical monophenyl cyclic 1,4-diazadienes with ketene derivatives yields new structures *via* 1,5-sigmatropic reactions. These structures were determined and confirmed by single-crystal X-ray analysis. The reaction mechanism was investigated by density functional theory calculations. The result of the calculation indicated whether the reaction was a cyclization reaction or a 1,5-shift rearrangement based on the stability of the intermediate conformation.

β- Lactam antibacterial drugs are antibiotics that have a common skeleton and can be classified into several groups depending on the structure that contacts the monobactam ring.[1] Following on from the successful elucidation of the β-lactam ring structure, various synthetic methods have been developed for its preparation,[2] with the [2+2] ketene–imine cycloaddition reaction having been described for some derivatives.[3] Indeed, our group has researched this addition reaction using dihydropyridine as a reaction substrate,[4] and we have elucidated the reaction mechanism of the reactivity based on molecular orbital (MO) calculations.

In a previous study,[5] the reaction of dihydropyrazines with ketene provided a range of β-lactam derivatives (1:1 and 1:2 adducts based on the reaction stoichiometry). Through X-ray crystallographic and MO calculations, this reaction was considered to be a stepwise pathway *via* betaine intermediates. Thus, we herein report the development of a synthetic route to the β-lactam ring structure with unsymmetrical monophenyl-dihydropyrazines and ketenes, and provide evidence for a stepwise reaction *via* betaine intermediates.

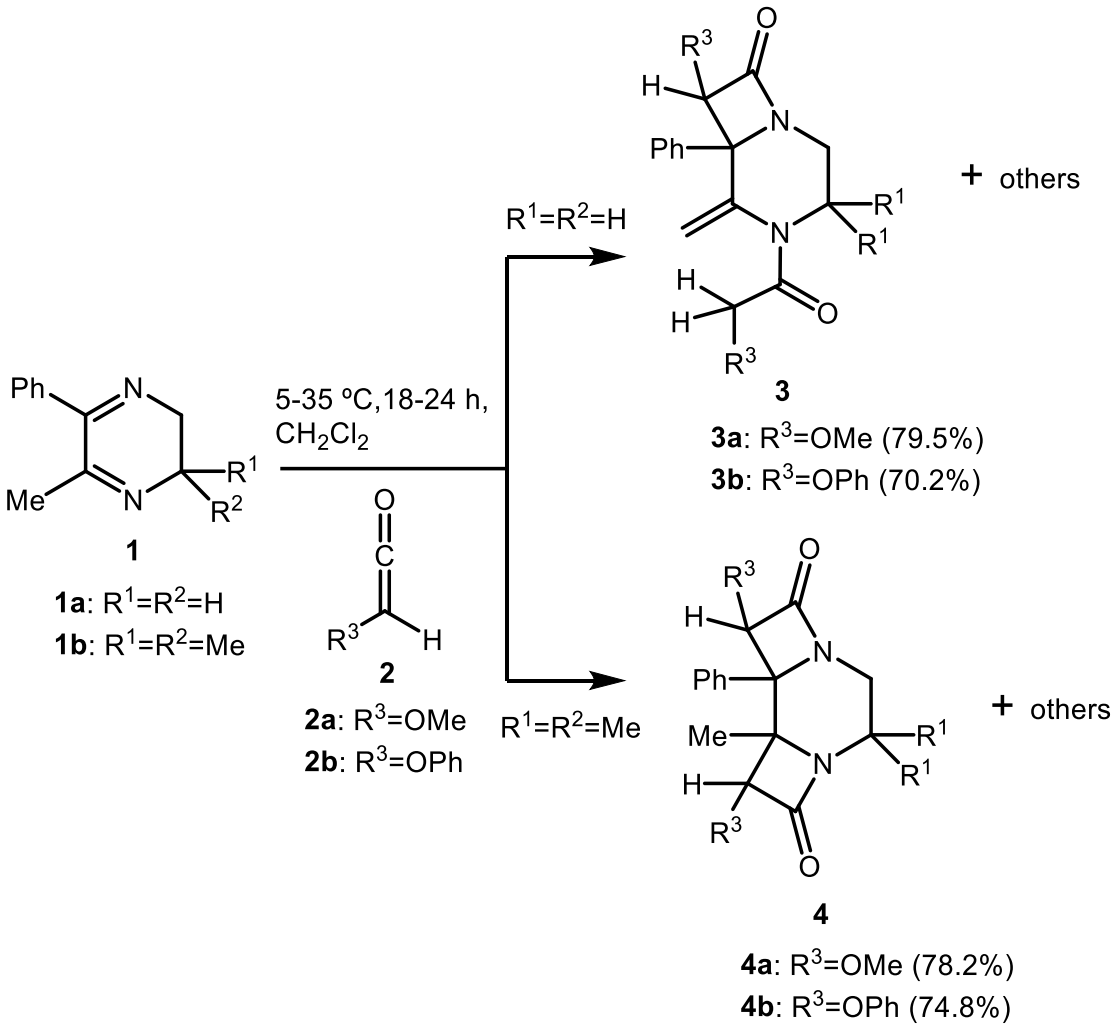

Figure 1. 1,5-Shift rearrangement and cyclization reactions for the reaction between cyclic 1,4-diazadienes and ketene

The reaction of 2,3-dihydro-6-phenylpyrazine derivatives (**1a**, **1b**) with ketenes (**2a**, **2b**) yielded β-lactam compounds **3** and **4**, where compound **3** contained a lactam skeleton, and compound **4** contained two lactam skeletons; the former of which was attributed to a hydrogen transfer rearrangement. In the ^{1}H NMR spectrum of **3a**, signals corresponding to methyl protons were observed at 3.03 and 3.22 ppm, while the methylene protons were represented at 3.03, 3.26, 3.47, 3.95, 4.10, 4.73, 5.42, and 5.54 ppm, and a methine proton was found at 4.89 ppm. Moreover, the ^{13}C NMR spectrum of **3a** indicated the presence of methyl carbon atoms (58.4 and 58.8 ppm), methylene carbon atoms (37.9, 45.0, 69.5, and 112.9 ppm), a methine carbon atom (92.2 ppm), a quaternary carbon atom (68.7 ppm), an alkene double bond (147.0 ppm), phenyl groups (127.0, 128.8, 128.9, and 133.9 ppm), and carbonyl carbon atoms (165.6 and 167.9 ppm). In addition, in the infrared spectrum of this compound, a typical absorption signal corresponding to the β-lactam carbonyl group was found at 1757 cm^{-1}. Furthermore, analysis by mass spectrometry showed a fragment peak at 316, attributed to M^{+}. Detailed assignment of the NMR data was performed by distortionless

enhancement by polarization transfer (DEPT), heteronuclear multiple quantum correlation (HMQC), heteronuclear multiple bond connectivity (HMBC), and ^{1}H-^{1}H correlation spectroscopy (COSY) (Table 1). Figure 2 shows the COSY spectrum of **3a**, which reveals a correlation between H5 (4.89 ppm) and H10 (5.54 ppm), corresponding to the hydrogen atom of the methine group in the β-lactam ring and the hydrogen atom of the methylene group. The signal at 5.54 ppm was a doublet signal (J=1.2 Hz), and was considered to be a long-range coupling. In addition, H8 (3.47 ppm) was highly shifted owing to the effect of the phenyl group; hence we conclude that this structure adopts an *anti*-type arrangement in which the two ketene fragments are positioned on opposite faces of the pyrazine ring, as shown on the left side of Figure 2. To confirm this structure, which was proposed on the basis of various spectral data, **3a** was subjected to single crystal X-ray analysis (right side of Figure 2). Moreover, the ^{1}H and ^{13}C NMR spectra of compounds **4a** and **4b**, containing two β-lactam rings, were analyzed according to the method described in a previous study.[5]

Table 1. NMR data for **3a**

Position No. *	^{13}C NMR	DEPT/HMQC	^{1}H NMR	HMBC
1	37.9	CH_2	3.26, 3.95	5, 6
2	45.0	CH_2	3.03, 4.73	1
3	147.0	C	-	10
4	68.7	C	-	10
5	92.2	CH	4.89	1, 6, 11
6	165.6	C	-	1, 5
7	167.9	C	-	8
8	69.5	CH_2	3.47, 4.10	9, 10
9	58.4	Me	3.03	8
10	112.9	CH_2	5.42, 5.54	3, 4, 8
11	58.8	Me	3.22	5

*Position No. relates to the structure shown in Figure 2.

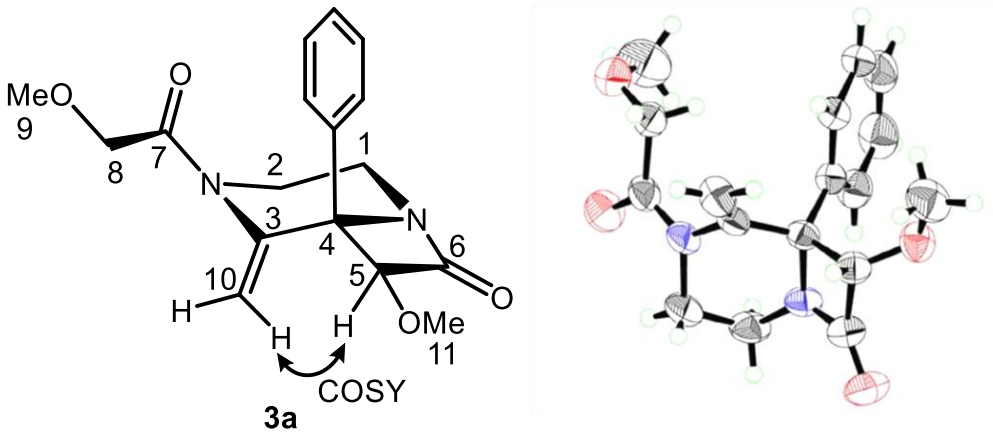

Figure 2. COSY correlation for the predicted structure of **3a** and the ORTEP diagram of **3a**

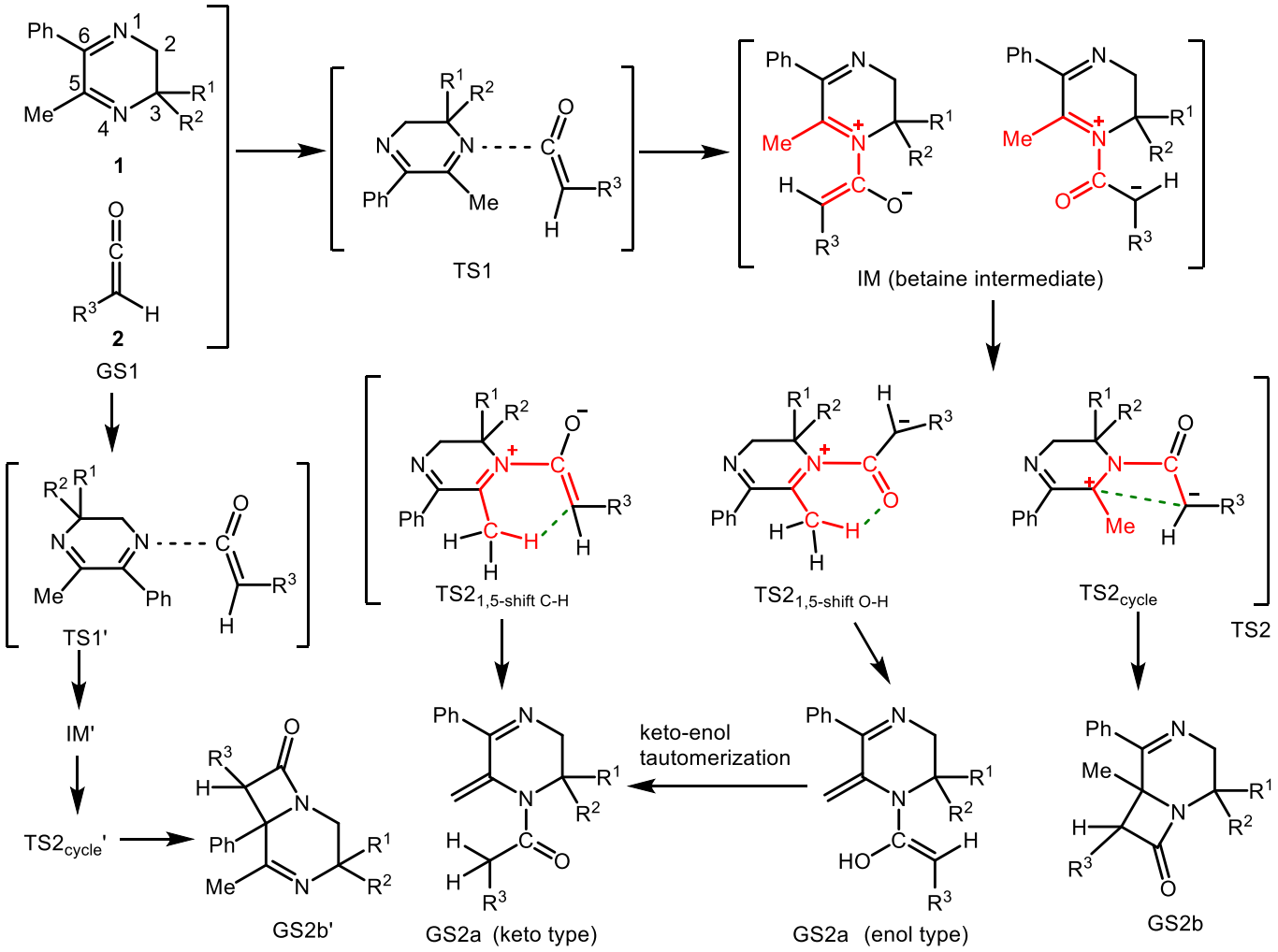

Figure 3. Proposed reaction mechanism

The obtained results indicated that the reaction of **1a** with ketenes **2a** and **2b** resulted in a rearrangement reaction, producing a 1,5-hydrogen shift product. In contrast, the reaction of **1b** with ketenes (**2a** and **2b**) resulted in a [2+2] cyclization reaction to give the β-lactam product, as before.[5] We predicted that this difference in reactivity was not influenced by the substituent on the ketene moiety, but was inferred to be due to the substituent at the third position of the 2,3-dihydro-6-phenylpyrazine derivative. Therefore, the reaction mechanism was analyzed to clarify the differences in the obtained products. Based on the two products recovered from this experiment (i.e., **3** and **4**), three possible routes exist, as outlined in Figure 3.[6,7] Firstly, the lone pair on the nitrogen atom of the pyrazine ring (reaction point; Me-C=N or Ph-C=N) reacts with the central carbon atom of the ketene to form the betaine intermediate (IM) *via* transition state 1 (TS1). Subsequently, transfer of the hydrogen of the methyl group at the fifth position of the 2,3-dihydro-6-phenylpyrazine derivative, or cyclization to form the lactam ring *via* $TS2_{cycle}$, are both possible. In terms of the hydrogen transfer reaction, two possible routes exist, namely the direct hydrogen transfer route *via* $TS2_{1,5\text{-shift C-H}}$, and a route *via* the oxygen anion originating from $TS2_{1,5\text{-shift O-H}}$. The ground state enol form

of **2a** (GS2a enol type), which was obtained by hydrogen transfer *via* the oxygen anion, then undergoes keto-enol tautomerization,[8,9] resulting in formation of the stable GS2a (keto type). TS calculations using the B3LYP6-31G(d)[10] level of theory were performed for the reaction of **1a** ($R^1 = R^2 = H$) with ketene ($R^3 = H$) without a substituent (Table 2). Similarly, TS calculations were performed for the reaction of **1b** ($R^1 = R^2 = Me$) with ketene ($R^3 = H$), again without a substituent (Table 2). The structure obtained from these TS calculations was later confirmed to be the true TS structure based on vibrational frequency analysis and intrinsic reaction coordinate calculations (IRC). The result of the vibrational frequency analysis confirmed that there is only one imaginary vibration. Furthermore, using IRC calculations, we confirmed that the primordial and generative systems are reached based on the only imaginary vibration obtained the vibrational frequency analysis.

Table 2. Calculated heats of formation for the reactants and products, and the energies of the transition state structures obtained using the B3LYP6-31G(d) level of theory

Reaction between **1a** and ketene						
State	1,5-Hydrogen shift C-H		1,5-Hydrogen shift O-H		Cycloaddition	
GS1	−688.04923	(0.0)	−688.04923	(0.0)	−688.04923	(0.0)
TS1	-	-	−688.04388	(3.36)	-	-
IM	-	-	−688.04425	(3.12)	-	-
TS2	−688.02108	(17.66)	−688.02346	(16.17)	−688.02155	(17.36)
GS2	−688.09867	(−31.02)	−688.05162	(−1.50)	−688.09831	(−30.80)
Reaction between **1b** and ketene						
State	1,5-Hydrogen shift C-H		1,5-Hydrogen shift O-H		Cycloaddition	
GS1	−766.62348	(0.0)	−766.62348	(0.0)	−766.62348	(0.0)
TS2	−766.58146	(26.37)	−766.58802	(22.25)	−766.59554	(17.53)
GS2	−766.66049	(−23.22)	−766.62067	(1.76)	−766.67146	(−30.11)

Relative energy (kcal/mol) in parentheses; ΔΔHf (kcal/mol) = (GS1 – each state of energy) ×627.5; 1 hartree = 627.5 kcal/mol.

In the reaction between **1a** and ketene, IRC analysis with optimization calculations at each point of the reaction pathway of the cyclization and the direct 1,5-hydrogen transfer (1,5-hydrogen shift C-H) pathway showed that TS1 could not be explored because of the lack of energy convergence of the IM, resulting in GS1 being the primordial system, and GS2a (keto type) or GS2b being the generative system. As a reference, semi-empirical methods[11] for finding the initial structure of the DFT method yielded the TS1 and IM structures for the AM1 and RM1 methods, but not for the PM7 method. The IM structure of the 1,5-hydrogen transfer process *via* the oxygen anion was stabilized, and its energy was found to converge in the IRC analysis. Therefore, we interpreted IM to be the primordial system and GS2a (enol type) to be the generative system in TS2, i.e., the latter part of the 1,5-hydrogen shift O-H reaction pathway. Moreover, the search for the TS1 between GS1 and IM, i.e., the former part of the reaction pathway, indicated that the

structures of TS1 and IM, which are key in this reaction, were likely stabilized by >C=O···H-C type interactions[12] between the oxygen atom of the ketone carbonyl group and the two hydrogen atoms of the methyl group at the fifth position of the 2,3-dihydro-6-phenylpyrazine derivative (Figure 4). We interpreted GS1 to be the primordial system and IM to be the generative system in TS1, i.e., the former part of the 1,5-hydrogen shift O-H reaction pathway. As shown by the energy values presented in Table 2, the 1,5-hydrogen shift pathway initially passed through TS1 to give the resulting stable IM; the energy of the IM was only 0.24 kcal/mol lower than that of TS1. Subsequently, IM transformed into TS2, which was found to be 13.05 kcal/mol higher in energy than IM. This reaction pathway had the lowest energy and was more expedient than the other two possible routes. Furthermore, this reaction pathway also represented the most thermodynamically stable process, since the energy of GS2a (enol type) was lower 1.5 kcal/mol lower than that of GS1. As for the reaction between ketene and the imine on the phenyl group side (Ph-C=N) as the reaction point, the energy of $TS2_{cycle}'$, the formation of which represents the rate-limiting step, reaches 19.42 kcal/mol, thereby indicating that the reaction with the imine on the methyl group side (Me-C=N) proceeds first.

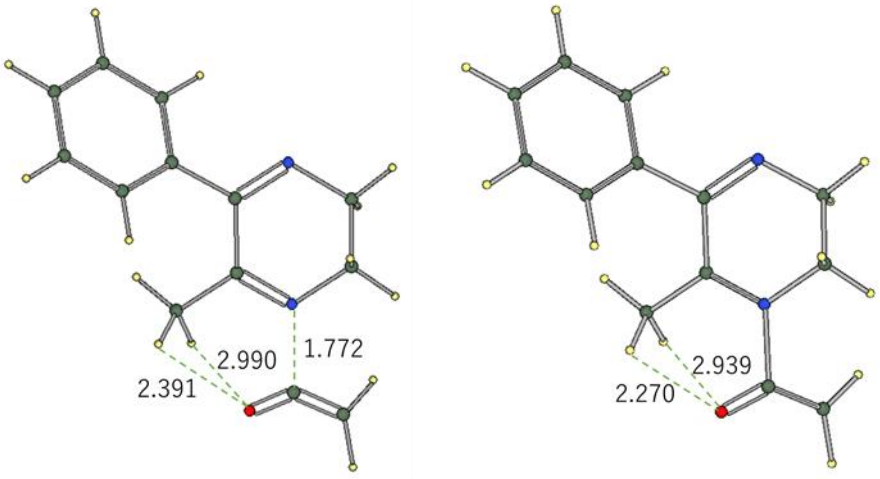

Figure 4. Interatomic distances (Å) between the carbon and nitrogen atoms forming the C-N bond in TS1, and the interatomic distances (Å) of the >C=O···H-C type interactions in the TS1 and IM structures resulting in the 1,5-hydrogen shift O-H pathway

In the reaction between **1b** and ketene, IM was unstable and a lack of energy convergence existed for all pathways, and so TS1 and IM were not obtained. As shown in Table 2, comparison of the reaction routes showed that the TS2 energy of the cyclization reaction was the lowest, while that energy of the GS2b product was the lowest. It was therefore considered likely that the cyclization reaction occurs here, both from a thermodynamic and a kinetic perspective. With respect to the 1,5-hydrogen shift, the energy of TS2

was 8.84 kcal/mol higher than that of the corresponding TS2 for the cyclization process. In addition, the energy of the product (GS2b) the from the 1,5-hydrogen shift was 1.8 kcal/mol higher than that of the GS1 product, and so these 1,5-shift hydrogen reactions were not expected to proceed. As for the reaction between ketene and the imine on the phenyl group side (Ph-C=N) as the reaction point, the energy of TS_{2cycle}', the formation of which represents the rate-limiting step, reaches 19.70 kcal/mol, thereby indicating that the reaction with the imine on the methyl group side (Me-C=N) proceeds first, as in the reaction between **1a** and ketene.

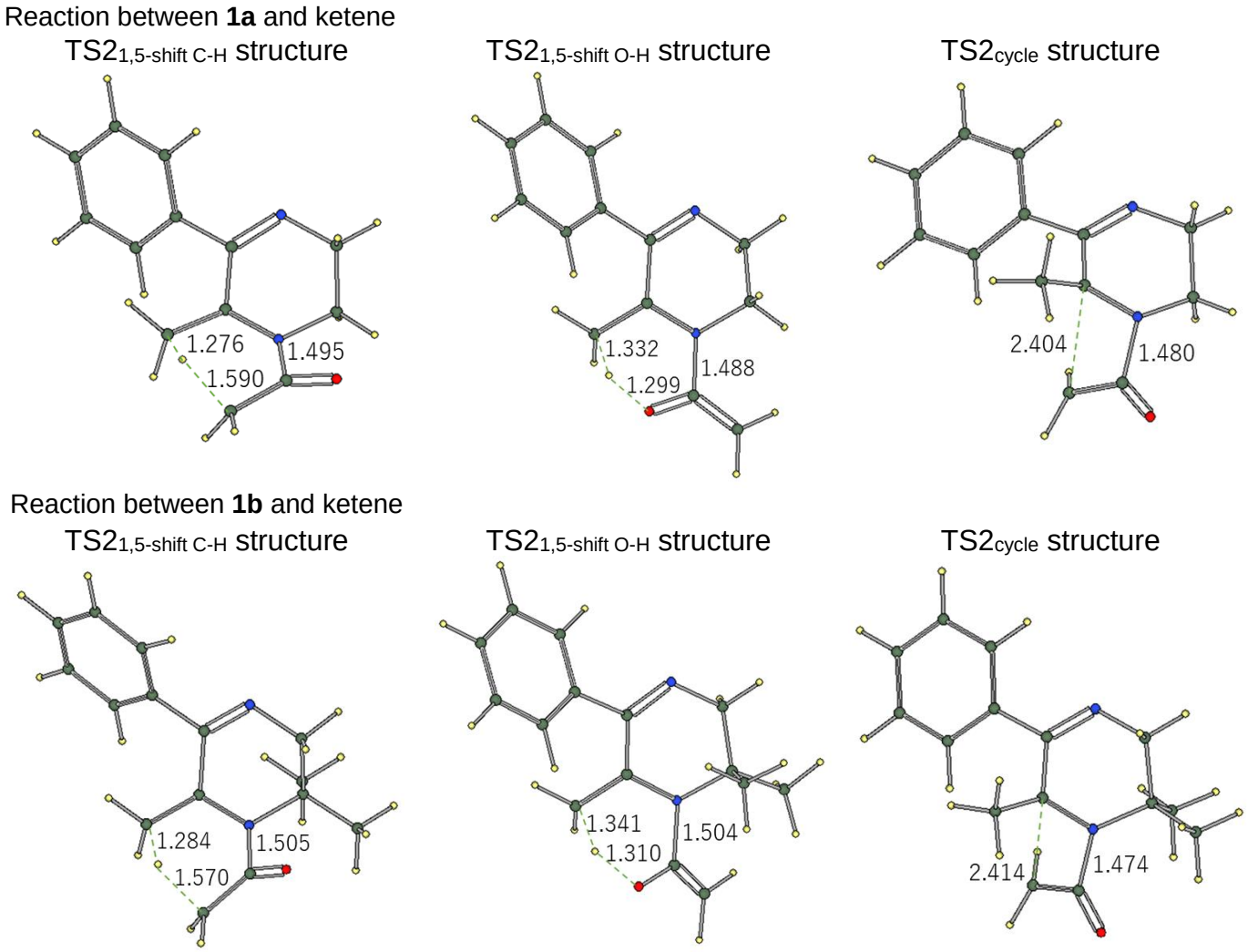

Figure 5. Interatomic distances (Å) between the carbon, oxygen and hydrogen atoms forming the C-H, O-H, and C-C bonds in the TS2 structure

The difference in the TS2 energies obtained for the reactions of **1a** and **1b** with ketene may be attributed to the dihedral angles, ∠C=N$^+$-C=C or ∠C=N$^+$-C=O, of the TS2 structures. To avoid the steric hindrance caused by the dimethyl group at the three position of the 2,3-dihydro-6-phenylpyrazine derivative, the

dihedral angles of the TS2 structures were shifted by ~20° (∠C=N$^+$-C=C changed from 30.21 to 50.60°, ∠C=N$^+$-C=O changed from 20.94 to 36.90°) for both 1,5-hydrogen shifts (i.e., C-H and O-H) (Figure 5). As a result, in the TS2 structure, the planarity created by the conjugated electron system could not be maintained and the energy was considered to increase. The dihedral angle ∠C=N$^+$-C=C of the TS2 structure for formation of the lactam ring remained almost unchanged, with only a slight increase from 36.14 to 37.27°.

As indicated in Table 3, two possible routes for keto-enol tautomerization exist,[8,9] and so both the direct intramolecular hydrogen shift and the water-assisted hydrogen shift were investigated. More specifically, the TS energy of the water-assisted hydrogen shift was 34.93 kcal/mol lower than that of the intramolecular hydrogen shift, indicating that the former reaction was more likely to proceed. From these calculation results, it was considered that the addition of water at the end of the reaction resulted in a conversion from GS2a (enol type) to the stable GS2a (keto type).

Table 3. B3LYP6-31G (d) energies (hartree) for the keto-enol tautomerization

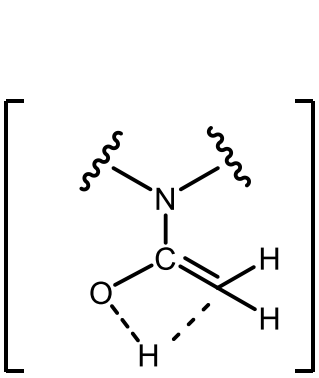

Intramolecular hydrogen shift

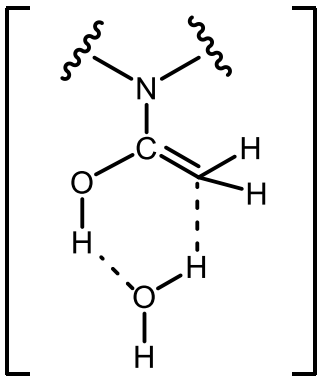

Water-assisted hydrogen shift

State	Intramolecular hydrogen shift		Water-assisted hydrogen shift	
GS2a (enol type)	−688.05162	(0.0)	−764.42345	(0.0)
TS tautomerization	−687.99080	(38.16)	−764.41831	(3.23)
GS2a (keto type)	−688.09867	(−29.52)	−764.47050	(−29.52)

Relative energies (kcal/mol) in parentheses; ΔΔHf (kcal/mol) = (Enol type product of energy – each state of energy) ×627.5; 1 hartree = 627.5 kcal/mol. H_2O: −76.37183 hartree. Part of the TS structure during the intramolecular hydrogen shift and water-assisted hydrogen shift, and interatomic distances (Å) between the oxygen and hydrogen atoms involved in the TS structure during the intramolecular hydrogen shift and water-assisted hydrogen shift.

In this study, the reaction of dihydropyrazine with ketene yielded not only lactam products **4** but also new products **3**. The structures of the new products were determined by NMR and X-ray analysis, and

computational analysis of the reaction revealed that following formation of the betaine intermediate, a 1,5-hydrogen shift reaction through the oxygen atom of the ketene occurred. A subsequent tautomerization reaction then took place to yield the new product. It was found that this reaction was influenced by the substituent present at the third position of the dihydropyrazine moiety, which forms a lactam structure in the presence of steric hindrance, but gives the 1,5-hydrogen shift product in the absence of steric hindrance. Current work in our group is focusing on determination of the structures of the minor products, in addition to reaction monitoring by HPLC. Future work will focus on the attempted synthesis of various derivatives to examine in further detail whether a β-lactam is obtained, or whether a 1,5-hydrogen shift takes place, and also to elucidate the reaction mechanism using kinetic isotope effects with deuterated **1a**.

EXPERIMENTAL

MATERIALS AND INSTRUMENTS

The reported melting points were uncorrected. The IR spectra were obtained using a Hitachi 270-30 spectrophotometer. ^{1}H NMR and ^{13}C NMR spectra were obtained on a JNM-ECA 500 (500 MHz) spectrometer using tetramethylsilane (TMS) as the internal standard. Mass spectra were obtained using a JMS-DX303HF instrument. Chemicals for the preparation of the cyclic 1,4-diazadienes and ketene were purchased from Wako Pure Chemical Industries, Ltd. The cyclic 1,4-diazadienes (**1a**, **1b**) were prepared according to the literature.[13] Since 2,3-dihydro-3,3,5-trimethyl-6-phenylpyrazine (**1b**) was obtained as a mixture (i.e., 2,3-dihydro-3,3,5-trimethyl-6-phenylpyrazine and 2,3-dihydro-2,2,5-trimethyl-6-phenylpyrazine; product ratio 10:1), and was used without separation. The identity of **1b** was confirmed by 2D NMR experiments, where the HMBC spectrum of **1b** revealed a correlation between the H2 hydrogen atom (CH_2, 3.55 ppm) and the C6 carbon atom (phenyl, 137.9 ppm). Ketenes **2a** and **2b** were also synthesized according to established methods.[5]

GENERAL EXPERIMENTAL PROCEDURE

Products **3** and **4** were synthesized according to the following procedure. A solution of methoxyacetyl chloride (0.43 g, 4 mmol) in CH_2Cl_2 (5.5 mL) was added dropwise to a solution of cyclic 1,4-diazadiene (2 mmol) in CH_2Cl_2 containing trimethylamine (0.55 mL). After stirring at 5–35 °C overnight, aqueous $NaHCO_3$ was added to neutralize the reaction mixture. The products were extracted with CH_2Cl_2 three times and dried over anhydrous $MgSO_4$. Following filtration, evaporation of the solvent gave the crude product, which was purified by chromatography using Et_2O and *n*-hexane on silica gel. Crystallization from *n*-hexane yielded the pure product.

3a: Colorless prisms. Yield 79.5%. mp 172–173 °C. IR (KBr) cm^{-1}: 1757 (C=O). ^1H NMR (500 MHz, $CDCl_3$) δ: 3.03 (1H, m, CH), 3.03 (3H, s, CH_3), 3.22 (3H, s, CH_3), 3.26 (1H, m, CH), 3.47 (1H, d, *J* =14.6 Hz, CH), 3.95 (1H, m, CH), 4.10 (1H, d, *J* = 14.6 Hz, CH), 4.73 (1H, brs, CH), 4.89 (1H, s, CH), 5.42 (1H, s, CH), 5.54 (1H, d, *J* = 1.2 Hz, CH), 7.34–7.43 (5H, m, aromatic-H). ^{13}C NMR (125 MHz, $CDCl_3$) δ: 37.9 (CH_2), 45.0 (CH_2), 58.4 (OCH_3), 58.9 (OCH_3), 68.7 (C), 69.5 (CH_2), 92.2 (CH), 112.9 (=CH_2), 121.1, 127.0, 128.8, 128.9, 133.9, 147.0 (>C=), 165.6 (C=O), 167.9 (C=O). EI-MS (*m/z*) 316 (M^+). *Anal*. Calcd for $C_{17}H_{20}N_2O_4$: C, 64.54; H, 6.37; N, 8.86: Found: C, 64.62; H, 6.38; N, 8.93.

The reaction of **1a** and **2b** yielded not only the 1:2 adduct (**3b**), but also a small amount of the 1:1 adduct.

1:1 adduct: Colorless prisms. Yield 6.5%. IR (KBr) cm^{-1}: 1750 (C=O). ^1H NMR (500 MHz, $CDCl_3$) δ: 2.39 (3H, s, CH_3), 3.26 (1H, m, CH), 3.50 (1H, m, CH), 3.63 (1H, m, CH), 3.92 (1H, m, CH), 5.36 (1H, s, CH), 6.90–7.51 (10H, m, aromatic-H). ^{13}C NMR (125 MHz, $CDCl_3$) δ: 24.9 (CH_3), 37.8 (CH_2), 44.9 (CH_2), 65.2 (C), 85.3 (CH), 116.7, 122.9, 127.7, 128.4, 128.6, 128.8, 129.7, 133.9, 157.2, 167.2 (C=N), 170.7 (C=O). EI-MS (*m/z*): 306 (M^+). *Anal*. Calcd for $C_{19}H_{18}N_2O_2$: C, 74.49; H, 5.92; N, 9.14: Found: C, 74.54; H, 5.96; N, 9.20.

3b: Colorless prisms. Yield 70.2%. IR (KBr) cm^{-1}: 1766 (C=O). ^1H NMR (500 MHz, $CDCl_3$) δ: 3.14 (1H, m, CH), 3.36 (1H, m, CH), 4.04 (1H, d, *J* = 13.4 Hz, CH), 4.18 (1H, d, *J* = 14.8 Hz, CH), 4.65 (1H, d, *J* = 14.8 Hz, CH), 4.80 (1H, brs, CH), 5.51 (1H, s, CH), 5.61 (1H, d, *J* = 1.7 Hz, CH), 5.62 (1H, s, CH), 6.35 (2H, s, aromatic-H), 6.84–7.80 (13H, m, aromatic-H). ^{13}C NMR (125 MHz, $CDCl_3$) δ: 38.0 (CH_2), 45.2 (CH_2), 64.7 (CH_2), 68.8 (C), 88.6 (CH), 114.8 (=CH_2), 116.2, 116.5, 122.0, 122.9, 127.2, 128.0, 128.4, 128.9, 129.5, 129.6, 129.8, 133.5, 133.7, 148.0 (>C=), 157.0, 157.7, 164.8 (C=O), 166.9 (C=O). EI-MS (*m/z*) 440 (M^+). *Anal*. Calcd for $C_{27}H_{24}N_2O_4$: C, 73.62; H, 5.49; N, 6.36: Found: C, 73.70; H, 5.52; N, 6.41.

4a: Colorless prisms. Yield 78.2%. mp 178–180 °C. IR (KBr) cm^{-1}: 1735 (C=O). ^1H NMR (500 MHz, $CDCl_3$) δ: 1.35 (3H, s, CH_3), 1.62 (3H, s, CH_3), 1.70 (3H, s, CH_3), 3.20 (1H, d, *J* = 13.4 Hz, CH), 3.21 (3H, s, CH_3), 3.39 (3H, s, CH_3), 3.81 (1H, d, *J* = 13.4 Hz, CH), 3.81 (1H, s, CH), 4.97 (1H, s, CH), 7.16–7.44 (5H, m, aromatic-H). ^{13}C NMR (125 MHz, $CDCl_3$) δ: 21.3 (CH_3), 26.0 (CH_3), 26.8 (CH_3), 48.8 (CH_2), 53.4 (C), 58.0 (OCH_3), 59.1 (OCH_3), 64.2 (C), 68.2 (C), 87.8 (CH), 88.5 (CH), 127.2, 128.2, 128.3, 136.5, 164.7 (C=O), 165.9 (C=O). Anal. Calcd for $C_{19}H_{24}N_2O_4$: C, 66.26; H, 7.02; N, 8.13: Found: C, 66.12; H, 7.10; N, 8.07. EI-MS (*m/z*) 344 (M^+).

4b: Colorless prisms. Yield 74.8%. mp 165–166 °C. IR (KBr) cm^{-1}: 1748 (C=O). ^1H NMR (500 MHz, $CDCl_3$) δ: 1.46 (3H, s, CH_3), 1.67 (3H, s, CH_3), 1.97 (3H, s, CH_3), 3.30 (1H, d, *J* = 13.4 Hz, CH), 3.90 (1H, d, *J* = 13.4 Hz, CH), 4.78 (1H, s, CH), 5.60 (1H, s, CH), 6.83–7.32 (15H, aromatic-H). ^{13}C NMR (125 MHz, $CDCl_3$) δ: 21.9 (CH_3), 26.1 (CH_3), 27.0 (CH_3), 48.9 (CH_2), 53.7 (C), 64.4 (C), 68.7 (C), 84.9 (CH), 85.3 (CH), 116.1, 116.6, 122.6, 127.6, 128.2, 128.4, 129.2, 129.5, 129.7, 135.4, 157.3, 163.6 (C=O), 164.9

(C=O). *Anal*. Caclcd for $C_{29}H_{28}N_2O_4$: C, 74.34; H, 6.02; N, 5.98: Found: C, 74.51; H, 6.03; N, 6.02. FAB-MS (*m/z*) 468 (M^+).

MOLECULAR ORBITAL (MO) CALCULATIONS

Semi-empirical MO calculations were performed using the Winmostar (GE) V4.105 interface[14] using MOPAC2016[11] on an Intel personal computer. Structures optimized using the semi-empirical methods were used as the starting geometries for the DFT calculations.[10] The energies were corrected using the zero-point vibrational energy (scaled by a factor of 1.000) computed at 298.15 K (GAMESS program default value). All data calculated at the B3LYP/6-31G(d) level of theory are available from the author upon reasonable request.

SINGLE-CRYSTAL X-RAY ANALYSIS

A colorless prism crystal with approximate dimensions of 0.400 × 0.400 × 0.400 mm was mounted on a glass fiber. All measurements were carried out on a Rigaku RAXIS RAPID imaging plate area detector using graphite monochromated Mo-Kα radiation. The data were collected at a temperature of 23±1 °C to a maximum 2θ value of 54.9°. The structures were solved by a direct method (SIR-2011),[15] and hydrogen atoms were placed in the calculation. A full-matrix least-squares technique was used with anisotropic thermal parameters for non-hydrogen atoms and a riding model for hydrogen atoms. All calculations were performed using the Crystal Structure crystallographic software package.[16,17] **3a**: $C_{17}H_{20}N_2O_4$, monoclinic, space group $P2_1/c$ (#14), a = 9.0672(15), b = 14.670(3), c = 12.6021(18) (Å), β (°) = 102.194(5), V = 1638.5(5) ($Å^3$), Density (calc.) 1.282, Density (obs.) 1.282 g cm^{-3}, Z = 4, R = 0.0617, Unique data used = 3663, Rw = 0.1367, and Goodness of Fit = 1.117. Crystallographic data were deposited at CCDC 2015173.

REFERENCES AND NOTES

1. K. Bush and P. A. Bradford, *Cold Spring Harb. Perspect. Med.*, 2016, doi: 10.1101/cshperspect.a025247.
2. C. R. Pitts and T. Lectka, *Chem. Rev.*, 2014, **114**, 7930.
3. S. Deketelaere, T. V. Nguyen, C. V. Stevens, and M. D'hooghe, *ChemistryOpen*, 2017, **6**, 301.
4. S. Oiso, M. Eto, Y. Yoshitake, and K. Harano, *Chem. Pharm. Bull.*, 2003, **51**, 1068.
5. K. Nakahara, K. Yamaguchi, Y. Yoshitake, T. Yamaguchi, and K. Harano, *Chem. Pharm. Bull.*, 2009, **57**, 846.
6. B. Alcaide, M. Miranda, J. Perez-Catells, C. Polanco, and M. A. Sierra, *J. Org. Chem.*, 1994, **59**, 8003.
7. C. Zhou and D. M. Birney, *J. Am. Chem. Soc.*, 2002, **124**, 5231.
8. S. Yamabe, N. Tsuchiba, and K. Miyajima, *J. Phys. Chem. A*, 2004, **108**, 2750.

9. M. A. Freitag, T. L. Pruden, D. R. Moody, J. T. Parker, and M. Fallet, *J. Phys. Chem. A*, 2007, **111**, 1659.
10. GAMESS, M. W. Schmidt, K. K. Baldridge, J. A. Boatz, S. T. Elbert, M. S. Gordon, J. J. Jensen, S. Koseki, N. Matsunaga, K. A. Nguyen, S. Su, T. L. Windus, M. Dupuis, and J. A. Montgomery, *J. Comput. Chem.*, 1993, **14**, 1347.
11. MOPAC2016, J. J. P. Stewart, Stewart Computational Chemistry, Colorado Springs, Co, USA, http://OpenMOPAC.net, 2016.
12. G. R. Desiraju and T. Steiner, The Weak Hydrogen Bond: In Structural Chemistry and Biology, Oxford University Press, 2001.
13. S. Ito, S. Takechi, K. Nakahara, N. Kashige, and T. Yamaguchi, *Chem. Pharm. Bull.*, 2010, **58**, 825.
14. Winmostar Version (GE) V4.105, X-Ability Co. Ltd., Tokyo, Japan, 2014.
15. SIR2011: M. C. Burla, R. Caliandro, M. Camalli, B. Carrozzini, G. L. Cascarano, C. Giacovazzo, M. Mallamo, A. Mazzone, G. Polidori, and R. Spagna, *J. Appl. Cryst.*, 2012, **45**, 357.
16. Crystal Structure 4.3: Crystal Structure Analysis Package, Rigaku Corporation (2000-2018). Tokyo 196-8666, Japan.
17. CRYSTALS Issue 11: J. R. Carruthers, J. S. Rollet, P. W. Betteridge, D. Kinna, L. Pearce, A. Larsen, and E. Gabe, Chemical Crystallography Laboratory, Oxford, U.K., 1999.